ACS Sustainable Chemistry & Engineering

pubs.acs.org/journal/ascecg

Research Article

CO_2 Separation Using Supported Deep Eutectic Liquid Membranes Based on 1,2-propanediol

Bartosz Nowosielski, Dorota Warmińska, and Iwona Cichowska-Kopczyńska*

Cite This: *ACS Sustainable Chem. Eng.* 2023, 11, 4093−4105

Read Online

ACCESS | Metrics & More | Article Recommendations | Supporting Information

ABSTRACT: In this work, deep eutectic solvents (DESs) composed of choline chloride, acetylcholine chloride or tetrabutylammonium chloride, and 1,2-propanediol were used as a liquid phase for polypropylene-based supported liquid membranes (SLMs) and evaluated for the separation of carbon dioxide from CO_2/N_2 mixtures. Fourier transform infrared spectra were obtained to confirm DES formation, and the thermal stability of solvents was investigated using thermogravimetric analysis. The physicochemical properties of DESs and carbon dioxide solubility were determined in a temperature range of 293.15−313.15 K. The effects of the hydrogen bond acceptor structure and the acceptor/donor molar ratio in regard to properties and CO_2 separation potential were discussed. The permeability of CO_2 and N_2 in DES-based SLMs was determined, and the ideal CO_2/N_2 selectivity was calculated. The gas permeation results of the 1,2-propanediol-based DES-based supported liquid membranes showed that the permeability of CO_2 varied from 86 to 152 barrers in 293.15 K. Similarly, the ideal CO_2/N_2 selectivity varied from 21 to 30. The performance of DES−SLMs was compared with the competing imidazolium-based supported ionic liquid membranes and proved DES−SLMs as a promising alternative considering their green potential and comparable gas separation performance.

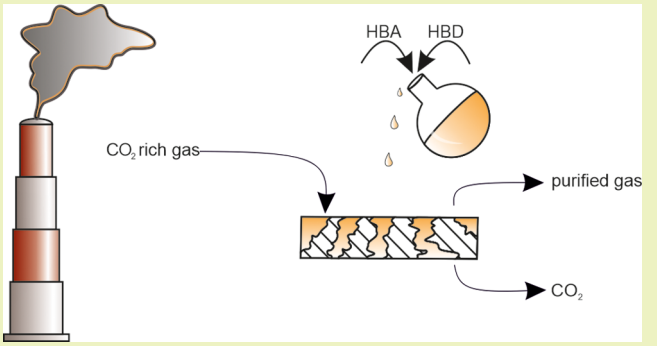

KEYWORDS: *deep eutectic solvents, supported liquid membranes, CO_2 separation, 1,2-propanediol*

INTRODUCTION

As global warming continues, new technologies are being sought to reduce emissions of carbon dioxide, which is one of the main greenhouse gases that also include water vapor, methane, volatile organic compounds, nitrous oxide, and ozone. The most important method proposed for this purpose is CO_2 capture and storage (CCS).[1] CCS technology involves capturing waste CO_2, transporting the captured CO_2 to a storage site and depositing it in a safe place. Although CO_2 deposition is currently considered the biggest problem in the process of carbon dioxide removal, its capture is not insignificant. So far, cryogenic distillation and absorption using aqueous alkanoamine solutions have been used at an industrial level for CO_2 capture.[2,3] However, both technologies used for carbon dioxide absorption have many disadvantages, such as high possibility of equipment corrosion and high energy consumption;[4] therefore, new technologies should be developed for this purpose. In recent years, membrane separation has been recognized as a cost-effective technology to reduce CO_2 emissions, and in addition to polymer-based membranes, supported liquid membranes (SLMs) have been introduced.[5] They are composed of polymeric support and liquid held in pores of support by capillary forces. The first liquids immobilized in a porous support for carbon dioxide separation were aqueous solutions of amines, and since 2002, ionic liquids (ILs) have been used and examined in gas separation.[6−8] It was found that supported ionic liquid membranes show high selectivity compared to the polymer membrane itself.[9] However, due to the high price, complex synthesis, and low biodegradability of ILs, their alternatives are still being sought. Most recently, deep eutectic solvents (DESs) have been used in SLM as a new substitute to ionic liquids[10−14] and their CO_2 capacity was proven.[15] DES-based SLMs have also become the subject of research in the field of olefin/paraffin separation, biotechnology, extraction, water purification, and energy processing and storage.[16−19]

In general, DESs consist of two components, namely, a hydrogen bond acceptor (HBA) and a hydrogen bond donor (HBD), and have similar physical properties to ionic liquids, are practically nonvolatile and nonflammable, and exhibit high

Received: October 20, 2022
Revised: February 17, 2023
Published: March 1, 2023

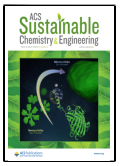

Table 1. Provenance and Mass Fraction Purity of the Compounds Studied

chemical name	$M/(g\cdot mol^{-1})$	source	CAS number	initial purity/mass fraction[a]	purification method	final purity/mass fraction[a]
choline chloride (ChCl)	139.62	Sigma-Aldrich	67−48−1	≥0.98	none	
acetylcholine chloride (AChCl)	181.66	Sigma-Aldrich	60−31−1	≥0.98	none	
tetrabutylammonium chloride (TBAC)	277.92	Sigma-Aldrich	1112−67−0	≥0.97	crystallization	≥0.98[b]
1,2-propanediol	76.09	Sigma-Aldrich	57−55−6	≥0.995	none	

[a]As stated by the supplier. [b]Determined by potentiometric titration.

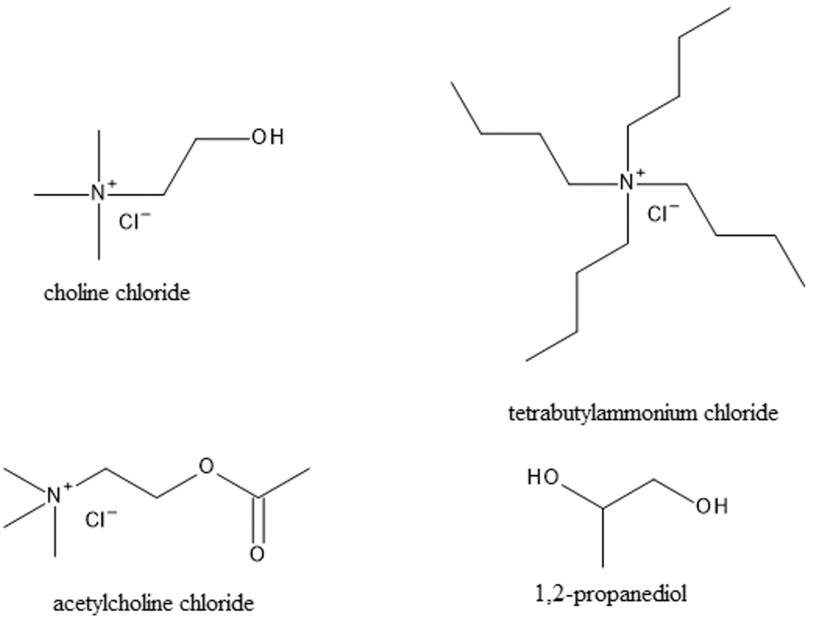

Figure 1. Chemical structures of chemicals used in this study.

thermal properties and electrochemical stability but are definitely cheaper, less toxic, and often biodegradable.[20]

To the best of our best knowledge, one the first DES-based SLMs for carbon dioxide separation has been reported by Amira et al.[21] The authors impregnated DES consisting of choline chloride (ChCl) and ethylene glycol (EG) (with a 1:3 molar ratio of HBA to HBD) into the polyvinylidenefluoride-*co*-polytetrafluoroethylene (PVDF-*co*-PTFE) polymer and used the obtained SLM for CO_2/N_2 separation. According to their results, ChCl-ethylene glycol DES/PVDF-co-PTFE SLM had a CO_2/N_2 ideal selectivity of 2.0. Ishaq et al. reported the permeation performance of poly(vinylidene difluoride) (PVDF) DES-based composite SLM in CO_2 separation. They found that among studied membranes, the SLMs containing DES based on monoethanolamine showed excellent selectivity of CO_2 equal to 70.47 and 78.86 for CO_2/CH_4 and CO_2/N_2, respectively.[13,22,23] Saeed et al. also examined supported liquid membrane based on PVDF, but in their research, they used DESs composed of betaine and urea/glycerol/ethylene glycol or DESs consisting of choline chloride and tartaric acid/malic acid/oxalic acid or DES based on potassium carbonate.[24−26] The authors showed that the separation factor CO_2/CH_4 for the studied SLMs was up to 60.16. Lian et al. incorporated an amino acid-based DES (L-arginine + ethylene glycol 1:5 molar ratio) to the PEBAX membrane at 5−20% g/g. The results showed that with the increase of DES loading the CO_2 permeability decreased, but the CO_2/N_2 selectivity increased up to 15% loading. For 15% DES loading, the selectivity increase reached 21% and the permeability loss was only 5%.[27] Craveiro et al. studied the poly(tetrafluoroethylene) (PTFE) membrane coated by choline chloride-based DESs with the addition of carbonic anhydrase.[14] They reported the highest CO_2 permeability for ChCl-urea (U)-based SLM and the highest CO_2/N_2 ideal selectivity for ChCl-glycerol based SLM. Castro et al. used choline chloride-levulinic acid to impregnate a PFTE membrane and investigated the effect of water on the permeation performance of this DES-based SLM in CO_2 separation.[28] They found that as the water content increased, both the permeability and the selectivity of CO_2/N_2 decreased.

In this work, it was the first time that deep eutectic solvents based on 1,2-propanediol were immobilized into a porous polypropylene support and evaluated for the separation of CO_2 from the CO_2/N_2 mixture. DESs were synthesized by mixing 1,2-propanediol with choline chloride, acetylcholine chloride, or tetrabutylammonium chloride, and Fourier transform infrared spectroscopy was studied to confirm the DES formation. The solubility of carbon dioxide in synthesized solvents and their physical properties, such as thermal stability, density, viscosity, and refractive index, were measured at a temperature range of 293.15−313.15 K. The effects of the hydrogen bond acceptor structure and the hydrogen bond acceptor/hydrogen bond donor molar ratio were discussed. Finally, the permeability of CO_2 and N_2 in DES-based SLMs was measured, and the ideal CO_2/N_2 selectivity was calculated and compared with competing high-performance imidazolium-based SILMs. The effect of operating conditions on membrane separation performance was also analyzed.

https://doi.org/10.1021/acssuschemeng.2c06278
ACS Sustainable Chem. Eng. 2023, 11, 4093−4105

Table 2. DES Specifications

symbol	HBA	HBA/HBD mole ratio	M_{DES}/(g·mol^{-1})	molar fraction[a] HBD	water content[b]
DES-A1	choline chloride	1:3.019	91.899	0.7512	0.00175
DES-A2	choline chloride	1:4.021	88.744	0.8008	0.00121
DES-B1	acetylcholine chloride	1:2.990	102.552	0.7493	0.00217
DES-C1	tetrabutylammonium chloride	1:2.987	126.713	0.7492	0.00234

[a]The standard uncertainty of the HBD molar fraction composition is 0.001. [b]Water content of DESs in mass fraction determined by the Karl–Fischer titration with the standard uncertainty ±0.0001.

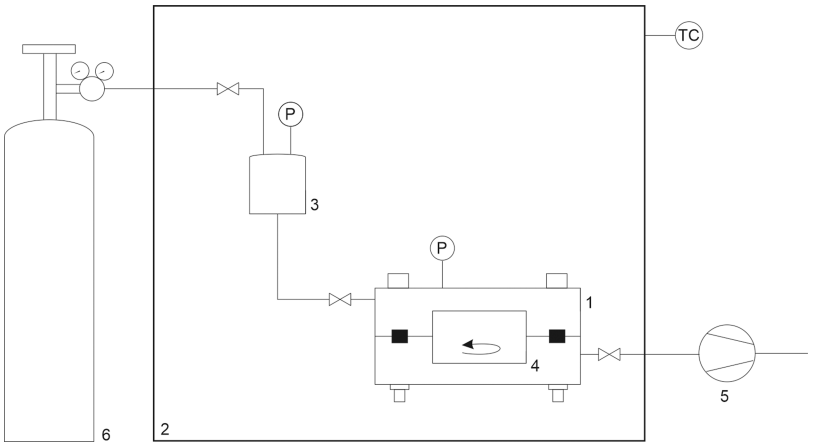

Figure 2. CO_2 experimental setup of gas solubility determination via isochoric saturation method (1, equilibrium cell; 2, thermostatic chamber; 3, intermediate gas tank; 4, magnetic stirrer; 5, vacuum pump; 6, gas tank).

EXPERIMENTAL SECTION

Materials. Table 1 presents the information about the chemicals used in this study, and in Figure 1 their chemical structures are presented. 1,2-Propanediol, choline chloride, acetylcholine chloride, and tetrabutylammonium chloride were purchased from Sigma-Aldrich (Saint Louis). Tetrabutylammonium chloride was purified by double crystallization from acetone by adding diethyl ether and the remaining chemicals were used as received from the producer. All salts were dried under reduced pressure before use for several days, choline chloride at 323.15 K and acetylcholine chloride and TBAC at 298.15 K. Polypropylene (PP) membranes with a pore size of 0.2 μm, a porosity of 80%, and a thickness of 9.3×10^{-5} m were obtained from Pall Corporation (New York). Carbon dioxide (0.9998 pure) and nitrogen (0.9998 pure) gases were supplied by Oxygen S.C. (Gdańsk, Poland).

Preparation of DESs. The DESs were prepared by mixing 1,2-propanediol with three different salts: choline chloride, acetylcholine chloride, and tetrabutylammonium chloride in a molar ratio of 1:3 HBA to HBD. For comparison, the DES-containing choline chloride in a molar ratio of 1:4 was also prepared. The preparation was carried out by mass using appropriate amounts of each DES component (Mettler Toledo with a precision of 0.00001 g) and mixed at 343.15 K for 1 h until a homogeneous liquid without any precipitate was formed. The obtained DESs, stable colorless liquids at room temperature, were kept in tight bottles to prevent any contamination that may affect the physical properties. Before experiments, the water content in DESs was determined by the Karl–Fischer method using a Mettler Toledo volumetric Karl–Fischer titrator (V10S). Table 2 presents its values along with the molar mass of DESs, their abbreviations, and the molar ratio and molar fraction of DES components.

Membrane Fabrication. The DES–SLMs were fabricated using the polypropylene porous support according to the well-known procedure described in the literature.[29−31] In the first step, both the DES and the polypropylene membrane were placed under vacuum at 323.15 K for 4 h to remove traces of gases and water from the pores. Thereafter, the polypropylene support was saturated with 0.1 cm^3 of DES per 1 cm^2 of the membrane. The excess liquid was removed with paper tissue, and the procedure was repeated until the weight of the membrane was stable. Then, the final mass of the liquid was compared to the theoretical calculations and if the saturation was close to 100% the membrane was used in separation experiments.

Thermogravimetric Analysis. The thermogravimetric analyses were performed using the TG 209F3 apparatus from Netzsch Group (Selb, Germany). Weighted samples (approx. 10 mg) were placed in a corundum dish. The measurement was carried out in an inert gas atmosphere-nitrogen with a flow rate of 50 mL·min^{-1} in the range from 298 to 1023 K at a heating rate of 10 K·min^{-1}.

Infrared Spectroscopy Measurements. FTIR experiments for liquid samples were performed using a Jasco-4700 instrument (4000–400 cm^{-1} with 32 scans, 4 cm^{-1} resolution; Jasco Company, Tokyo, Japan). Thin film method using salt (KBr) plates was applied by placing 1 drop of the solution on one salt plate. The spectrum from a clean plate was recorded as a background, and analysis of spectra was performed using Spectra Analysis software (Jasco Company, Tokyo, Japan). Spectra of solid samples (substrates) were recorded using dry salt KBr. The materials (1 mg) were compressed with potassium bromide (99 mg) to form a disc. Analysis were performed at 298.15 ± 0.1 K.

Density, Viscosity, and Refractive Index Measurements. The densities of the DES samples were obtained at different temperatures using a digital vibration-tube analyzer (Anton Paar DSA 5000, Austria) with a proportional temperature control that kept the samples at working temperature with an accuracy of ±0.01 K. The calibration was carried out using double-distilled, deionized, and degassed water and dry air at atmospheric pressure (0.1 MPa). The standard uncertainty of the density measurement was better than 0.1 kg·m^{-3}.

The viscosities of the DESs were measured with an LVDV-III Programmable Rheometer (cone-plate viscometer; Brookfield Engineering Laboratory), controlled by a computer. The temperature of the samples was controlled within ±0.01 K using a thermostatic water bath (PolyScience 9106). The display of the viscosimeter was verified with the certified viscosity standard N100 and S3 provided by Cannon at 298.15 ± 0.01 K. The standard uncertainty of viscosity measurement was better than 2%. At least three independent

https://doi.org/10.1021/acssuschemeng.2c06278
ACS Sustainable Chem. Eng. 2023, 11, 4093−4105

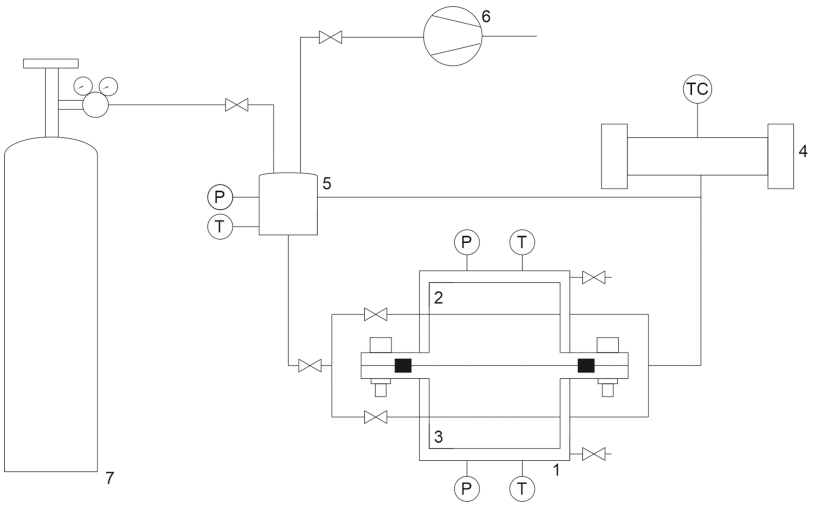

Figure 3. Experimental setup for gas permeation measurements (1, permeation chamber; 2, feed space; 3, permeate space 4, thermostat; 5, intermediate gas tank; 6, vacuum pump; 7, gas tank).

measurements were taken for each sample at each temperature to assure reproducibility of the measurement.

The refractive indices were obtained with an Abbe refractometer (RL-3, Poland) equipped with a thermostat for controlling the cell temperature with an accuracy of ±0.1 K. The standard uncertainty of refractive index measurement on the n_D scale was 0.0002. At least three independent measurements were taken for each sample at each temperature to assure reproducibility of the measurement.

Gas Solubility Measurement. The experimental setup for measuring CO_2 solubility using the isochoric saturation method is presented in Figure 2. The setup included an intermediate gas tank (3) and an equilibrium cell (1) equipped with a pressure sensor and a magnetic stirrer (4). The volume of the cell was 7.8 ± 0.01 cm^3. The individual parts were separated by gas-tight valves, and the system was placed in a thermostated tank (2) controlled by an LS thermostat (PolyScience 9106, Warrington, PA). The experimental uncertainty for the temperature was ±0.1 K.

Prior to the experiment, 1 cm^3 of liquid was placed in the equilibrium cell (1). A vacuum was applied in the system using a vacuum oil pump (5). After that, the intermediate gas tank (3) was filled with the gas (6). When the temperature was stable, the gas was introduced to the cell and initial pressure was recorded. The pressure was recorded continuously with an Aplisens PC-28 transducer with a standard uncertainty of 0.6 kPa, and the experiment was stopped when the equilibrium was reached, i.e., when the pressure in the system did not change for 1 kPa over 24 h. After reaching an equilibrium, another portion of CO_2 was injected into the equilibrium cell from the intermediate gas tank.

Validation of the method was conducted by measuring CO_2 solubility in water at 293.15 K, and the results were compared with the values reported in the literature.[32] The results are presented in Figure S1. A good agreement of data was obtained.

Gas Permeability Measurement. The laboratory setup for permeability measurements is presented in Figure 3 and was constructed in the Department of Process Engineering and Chemical Technology. The main part of the system was a permeation chamber equipped with a water coat (1) and divided into feed (2) and permeate (3) side. Intermediate gas reservoir (5) was placed in a thermostated tank (4) in which the constant temperature was maintained by means of an LS thermostat (PolyScience 9106, Warrington, PA) with an accuracy of ±0.1 K. Additional temperature Pt100 sensors were located in both parts of the membrane cell.

At the start of the experiment, vacuum was applied in the system using a vacuum oil pump (6). Then, gas reservoir (5) was filled with CO_2 or N_2 from the gas tank (7). When the temperature in the system was constant, the gas was delivered into the feed space. The initial gas pressure was about 22 kPa chosen experimentally to prevent from mechanic deformation and degradation of the membrane. The pressure in both chambers was recorded with a frequency of 0.1 Hz.

Theory. In this study, the amount of carbon dioxide dissolved in the DES was calculated by the following equation

$$n = n_0 - n_1 \tag{1}$$

where n_0 is the amount of carbon dioxide introduced to the measurement chamber and n_1 is the amount of CO_2 in the gas phase at equilibrium state.

The amount of CO_2 was obtained from eq 2

$$n_i = \frac{p_i V}{Z_2 RT} \tag{2}$$

where V is the volume of the gas phase in the cell in cm^3 (head space volume over DES corresponds to the chamber volume minus the volume of injected DES), p_i is the partial pressure in kPa (the initial or at equilibrium, respectively), R is the universal gas constant in $J \cdot mol^{-1} \cdot K^{-1}$, T is temperature in K, and Z_2 is the compressibility factor, which for ideal gases equals 1.

Since there is a physical absorption of carbon dioxide in DESs containing 1,2-propanediol, the solubility of CO_2 was used to calculate Henry's constant based on mole fraction (H_x) as follows[33]

$$H_x(p, T) \equiv \lim_{x_2 \to 0} \frac{p y_2 \phi_2(p, T, y_2)}{x_2} \tag{3}$$

Due to negligibly small vapor pressures of deep eutectic solvents, y_2 can be simplified to be unity.[34] Additionally, at low CO_2 pressures, the fugacity coefficient of CO_2 is also close to 1;[35] therefore, eq 3 is simplified to

$$H_x(p, T) = \frac{p}{x_2} \tag{4}$$

Thus, in this work, Henry's constant was determined from the slope of the isothermal linear fit of equilibrium pressure versus mole fraction of CO_2.

The gas permeation in DES−SLM was calculated in barrers on the basis of the pressure difference between the feed and permeate side over the selected time period providing that the pressure drop was linear

$$P = 10^{10} \frac{V_n l}{At(p_{i,f} - p_{i,p})} \tag{5}$$

where l is the thickness of the membrane in cm, A is the membrane area in m^2, t is time in s, V_n is the volume of permeated gas at normal

https://doi.org/10.1021/acssuschemeng.2c06278
ACS Sustainable Chem. Eng. 2023, 11, 4093−4105

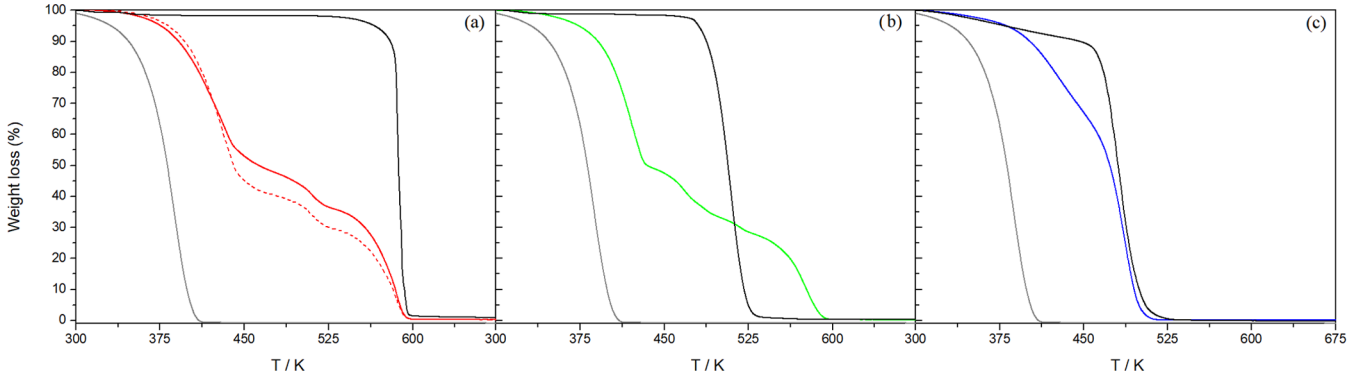

Figure 4. TGA curves obtained by thermogravimetry of DESs: (a) red straight line, ChCl:1,2-propanediol 1:3 (DES-A1); red dashed line, ChCl:1,2-propanediol 1:4 (DES-A2); (b) green straight line, AChCl:1,2-propanediol 1:3 (DES-B1); and (c) blue straight line, TBACl:1,2-propanediol 1:3 (DES-C1); black solid, salt; gray, 1,2-propanediol.

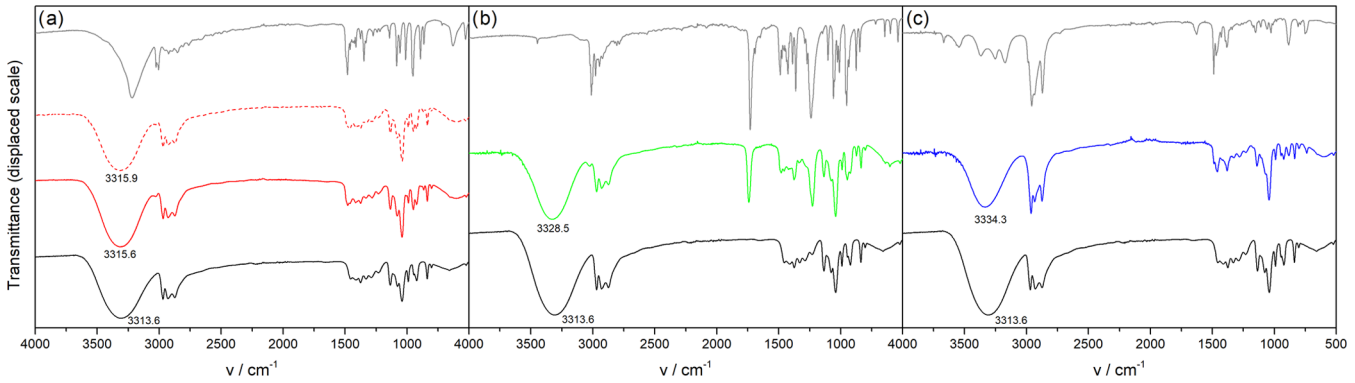

Figure 5. FTIR spectra for DES studied: (a) DES-A1 (red straight line) and DES-A2 (red dashed line), (b) DES-B1 (green straight line) and (c) DES-C1 (blue straight line); black straight line, neat 1,2-propanediol; gray straight line, salts.

conditions in cm^3, $p_{i(f)}$ and $p_{i(p)}$ are the pressure in mmHg of i in feed (f) and permeate (p), respectively.

The ideal CO_2/N_2 selectivity of the CO_2 over N_2 was calculated using the following equation

$$\alpha_{CO_2/N_2} = \frac{P_{CO_2}}{P_{N_2}} \tag{6}$$

where P_{CO_2} and P_{N_2} are the permeability of carbon dioxide and nitrogen, respectively.

RESULTS AND DISCUSSION

Characterization of DESs: Their Thermal Stability, FTIR Spectra, and Physical Properties. The knowledge of the physical properties of solvent, including its thermal stability, is crucial for every industrial and chemical process design, not just for CO_2 capture. Density is essential in many thermodynamic calculations as well as in the design and sizing of process equipment. Viscosity is important because it affects mass transport phenomena and conductivity of ionic fluids, thus affecting their suitability for specific applications. Moreover, it strongly influences the diffusion of dissolved particles in the solvent. Refractive index is an elemental property, which can be used for a component's identification, concentration determination, and purity confirmation.

Figure 4 presents TGA curves, i.e., the weight loss measured in % against temperature, for the studied DESs along with their pure components. As can be seen, for TBAC:1,2-propanediol (DES-C1), the curves consist of two steps: the first shows 1,2-propanediol decomposition and the second corresponds to the degradation of the salt. For acetylcholine chloride- and choline chloride-based DESs, an additional step is observed. The stability of all DESs is in between that of their components, and the order of stability is 1,2-propanediol < DES <salt. However, the complete decomposition of AChCl:1,2-propanediol (DES-B1) occurs at temperature higher than the neat AChCl. For DESs with the same molar ratio of HBA to HBD, the initial decomposition temperature measured as a 10% weight loss ($T_{10\%}$) changes according to the order: TBAC:1,2-propanediol (401.9 K) > ChCl:1,2-propanediol (391.5 K) > AChCl:1,2-propanediol (390.9 K). This sequence is consistent with the results obtained for phosphonium-based DES, showing that the thermal stability of DES increases with increasing length of the alkyl chain length of its components and is higher for systems with stronger hydrogen bond interactions.[36] Since the thermal stability of ChCl:1,2-propanediol (391.5 K) at a molar ratio of HBA to HBD 1:3 is lower than at a molar ratio of 1:4 (396.8 K), it can be suspected that in DES based on choline chloride with a higher content 1,2-propanediol, stronger interactions of hydrogen bonds take place. Summarizing, the obtained results of thermal analysis indicate that the studied DESs are suitable for using in the operating conditions for CO_2 capture.

The FTIR spectra of the studied DESs are presented in Figure 5 together with the spectra of neat 1,2-propanediol, choline chloride, acetylcholine chloride, and tetrabutylammonium chloride.

Regarding choline chloride (Figure 5a), the vibrational bands at 3219 and 3005−3025 cm^{-1} correspond to the

https://doi.org/10.1021/acssuschemeng.2c06278
ACS Sustainable Chem. Eng. 2023, 11, 4093−4105

Table 3. Physical Properties of DESs[a]

DES	T/K	ρ/kg·m^{-3}		η/mPa·s		n_D		f_m[e]/cm^3·mol^{-1}
		Exptl.	Lit.	Exptl.	Lit.	Exptl.	Lit.	
DES-A1 (ChCl:1,2-propanediol 1:3)	293.15	1071.82	1071.82[b], 1071.70[c]	83.79	94.05[b], 89.383[c]	1.4604	1.46137[c]	68.86
	298.15	1068.48	1068.76[b], 1068.62[c], 1069[d]	62.78	72.10[b], 68.432[c], 64.14[d]	1.4592	1.45995[c]	69.16
	303.15	1065.68	1065.71[b], 1065.54[c], 1066[d]	48.12	56.26[b], 53.339[c], 50.22[d]	1.4580	1.45853[c]	69.44
	308.15	1062.61	1062.65[b], 1062.47[c]	37.31	44.50[b], 42.261[c]	1.4565	1.45708[c]	69.71
	313.15	1059.55	1059.60[b], 1059.39[c], 1060[d]	29.17	35.89[b], 33.925[c], 31.92[d]	1.4552	1.45561[c]	70.00
	318.15	1056.48	1056.56[b], 1056.32[c]	23.43	29.15[b], 27.714[c]	1.4541	1.45418[c]	70.28
	323.15	1053.41	1053.48[b], 1053.24[c], 1054[d]	19.20	24.25[b], 22.880[c], 21.61[d]	1.4529	1.45275[c]	70.58
	328.15	1050.34	1050.41[b], 1050.16[c]	15.89	20.01[b], 19.111[c]	1.4516	1.45131[c]	70.85
	333.15	1047.27	1047.35[b], 1047.07[c], 1047[d]	13.37	17.11[b], 16.179[c], 14.92[d]	1.4503	1.45012[c]	71.15
DES-A2 (ChCl:1,2-propanediol 1:4)	293.15	1066.23	1065.56[b]	70.12	80.19[b]	1.4561		62.24
	298.15	1063.08	1062.43[b]	51.12	61.49[b]	1.4546		62.49
	303.15	1059.93	1059.28[b]	38.68	47.74[b]	1.4532		62.70
	308.15	1056.77	1056.12[b]	30.32	37.47[b]	1.4518		62.95
	313.15	1053.61	1052.97[b]	24.67	30.40[b]	1.4501		63.19
	318.15	1050.44	1049.70[b]	20.20	24.70[b]	1.4490		63.42
	323.15	1047.23	1046.63[b]	16.65	20.43[b]	1.4475		63.66
	328.15	1044.08	1043.50[b]	13.76	17.00[b]	1.4459		63.91
	333.15	1040.89	1040.28[b]	11.50	14.43[b]	1.4443		64.16
DES-B1 (AChCl-1,2-propanediol 1:3)	293.15	1081.99		90.49		1.4592		60.78
	298.15	1078.67		65.29		1.4575		61.03
	303.15	1075.37		48.79		1.4561		61.27
	308.15	1072.06		38.18		1.4548		61.51
	313.15	1068.77		29.87		1.4534		61.77
	318.15	1065.47		23.90		1.4520		62.00
	323.15	1062.18		19.98		1.4505		62.26
	328.15	1058.88		17.54		1.4494		62.52
	333.15	1055.59		13.82		1.4478		62.78
DES-C1 (TBAC-1,2-propanediol 1:3)	293.15	975.85		158.59		1.4604		94.26
	298.15	972.59		113.17		1.4588		94.68
	303.15	969.32		83.57		1.4571		95.11
	308.15	966.06		63.41		1.4555		95.54
	313.15	962.80		48.39		1.4540		95.97
	318.15	959.54		37.05		1.4525		96.40
	323.15	956.28		29.48		1.4508		96.84
	328.15	953.03		23.94		1.4492		97.28
	333.15	949.76		19.64		1.4479		97.71

[a]Standard uncertainties are $u(T) = 0.01$ K, $u(p) = 0.001$ MPa, $u(\rho) = 0.1$ kg·m^{-3}, $u(n_D) = 0.0002$, and $u(\eta) = 2\%$. [b]ref 42. [c]ref 41. [d]ref 40. [e]Free volume, f_m, calculated on the basis of experimental values of density and refractive index of DES. The details of the calculations are in the SM.

https://doi.org/10.1021/acssuschemeng.2c06278
ACS Sustainable Chem. Eng. 2023, 11, 4093−4105

presence of a hydroxyl group and an alkyl group, respectively, while the bands at 1205−885 cm^{-1} represent C−N vibrations.[37] Since acetylcholine chloride does not have a OH group, its spectrum (Figure 5b) does not show the vibrational band associated with this group, but it does show a different band at 1731 cm^{-1} characteristic for the C═O stretching vibrations.[38] In the spectrum of tetrabutylammonium chloride, the characteristic bands related to the presence of CH_3 and CH_2 groups were identified at 2958 and 2873 cm^{-1}. Moreover, an additional vibrational band in the range of 3367−3173cm^{-1} was observed, probably due to the water absorbed during the experiment, as TBAC is a highly hygroscopic material.[39] The band in the 1,2-propanediol spectrum represents a typical region of the ν(OH) stretching vibration range, particularly sensitive to hydrogen bonds located at 3314 cm^{-1}.

For the studied DESs, the spectra did not show any changes in the position of the bands and the formation of any new bonds in the relation to the spectra of pure salts. Thus, they confirm the lack of specific chemical interactions between DES components. Almost the only effect in the DES spectrum is the shift of the OH band position to the blue due to the appearance of the new OH-halide hydrogen bonds. The largest shift observed for DES-C1 suggests the strongest interactions between DES components, while the smallest shift obtained for DES-A1 implies the weakest interactions.

The density, viscosity, and refractive index of the deep eutectic solvents studied were measured as a function of temperature in the range of 293.15−333.15 K at ambient pressure, and their values are presented in Table 3 and Figure S2a−c. The literature data only available for choline chloride-1,2-propanediol (DES-A1 and DES-A2) is included in Table 3. As seen, the experimental values of density and refractive index are in good agreement with the values reported by other groups.[40−42] However, in the case of viscosity, there was a significant difference in the data compared to the literature, mainly due to the different water content and the different measurement method. It is worth noting that for the same reasons, the literature data differs remarkably from each other.

For all DESs studied, the density, refractive index, and viscosity decrease with the increase of temperature. Moreover, for the density and the refractive index, a linear relationship with temperature is observed, while the viscosity drops exponentially with temperature, as can be seen in Figure S2.

The fitting parameters of empirical linear equations correlating the effect of temperature on the density and refractive index ($y = a \cdot T + b$), obtained by least-squares analysis, are listed in Table 4. Very low RMSD values and R^2 values close to unity confirm the good linear dependence of these properties on temperature, as can be seen in Figure S2.

Table 5 shows the parameters derived from the experimental dynamic viscosity data that were fitted to the Vogel−Fulcher−Tamman (VFT) equation, which, as known from the literature, describes the viscosity−temperature relationship better than the Arrhenius equation.[20] The VFT equation is given as

$$\eta = \eta_o \exp^{b/T - T_o} \quad (7)$$

where η_0, b, and T_o are the fitting parameters, and T is the temperature in Kelvin.

Since 1,2-propanediol was common to all DESs, differences in the physical properties of the DES are due to the hydrogen bond acceptor and the interaction forces between HBA and glycol.

Table 4. Parameters of the Models of Density and Refractive Index along with Root-Mean-Square Deviations

DES	a	b	RMSD	R^2
		d/kg·m^{-3}		
DES-A1	−0.611	1250.82	0.088	0.9999
DES-A2	−0.633	1252.01	0.021	0.9999
DES-B1	−0.660	1275.42	0.010	1.0000
DES-C1	−0.652	1167.01	0.005	1.0000
		n_D		
DES-A1	−0.00025	1.5345	$0.9 \times 10-^4$	0.9993
DES-A2	−0.00029	1.5416	1.3×10^{-4}	0.9990
DES-B1	−0.00028	1.5410	1.2×10^{-4}	0.9989
DES-C1	−0.00031	1.5526	1.0×10^{-4}	0.9994

Table 5. Fitting Parameters for the Vogel−Fulcher−Tamman (VFT) Equation for Dynamic Viscosity Results Determined within the Temperature Range T = (293.15−333.15) K and P = 0.1 MPa

DES	η_0/mPa·s	b/K	T_0/K	RMSD	R^2
DES-A1	0.0277	1067.4	160.0	0.189	0.9999
DES-A2	0.3200	440.8	211.3	0.316	0.9997
DES-B1	0.3538	445.0	212.8	0.424	0.9997
DES-C1	0.0267	1093.4	167.3	0.412	0.9999

At the fixed temperature and the molar ratio of HBA to HBD, the density of the studied DESs is in the following order: AChCl:P (DES-B1) > ChCl:P (DES-A1) > TBAC:P (DES-C1). The higher density for choline chloride-based DES compared to the density tetrabutylammonium chloride-based DES was also reported for deep eutectic solvents containing p-toluenesulfonic acid as HBD.[43] According to the literature, the density decreases with increasing the length/symmetry of the cation-alkyl chain in DES because the elongation of the alkyl chain length increases the free volume of solvent. This is in line with our results because, as shown in Table 3, the TBAC-based DES has the highest free volume and the lowest AChCl:P (DES-B1).

The size of the solvent has also been found to affect its viscosity, and it has been observed that larger HBD or HBA results in higher DES viscosity.[44] In the present work, this phenomenon is visible in the TBAC:P (DES-C1) viscosity, which shows the highest values among the studied DES, regardless of the temperature. The viscosities of AChCl:P (DES-B1) and ChCl:P (DES-A1) show much lower values, indicating that the alkyl chain length of the salt has a greater effect on DES viscosity than the presence of an additional acetyl group in HBA. Taking into account the amount of 1,2-propanediol, the viscosity decreases when the ratio of HBA and HBD is lower. Obviously, the viscosity values of the studied DESs are also a result of the presence of hydrogen bonds, electrostatic, and van der Waals interactions between the individual components of DESs, which lead to an increase in flow resistance.

With regard to the refractive index of DESs, the order of ChCl:P (DES-A1) > TBAC:P (DES-C1) > AChCl:P (DES-B1) suggests that the ChCl is the most favorable enhancing HBA of refractive index, while AChCl is the lowest. This observation is somewhat surprising as it has been observed that the denser the liquid, the higher the refractive index.[45] Thus,

https://doi.org/10.1021/acssuschemeng.2c06278
ACS Sustainable Chem. Eng. 2023, 11, 4093−4105

many factors must determine the refractive index, not only the free volume as in the case of density, but also, i.e., the electronic polarizability of the DES molecule.

As seen from Table 3 and Figure S2, all physical properties of DESs depend on the HBA:HBD molar ratio. For ChCl-based deep eutectic solvent, both the density, refractive index, and viscosity decrease with the increasing of molar ratio of 1,2-propanediol. Obviously, this is the result of the relation of these properties for DESs and glycol. The densities, refractive indices, and viscosities for ChCl:P (DES-A1-A2) are higher than for neat 1,2-propanediol. Thus, as the amount of glycol in DES increases, the properties, tending to lower properties of pure 1,2-propanediol, decrease.

Solubility of Carbon Dioxide and Henry's Constant. The solubility of CO_2 in the studied deep eutectic solvents was measured in the temperature range of 293.15−313.15 K and pressures of 18−256 kPa. The solubility results at 298.15 K are shown in Figure 6. Table S1 presents the gas equilibrium

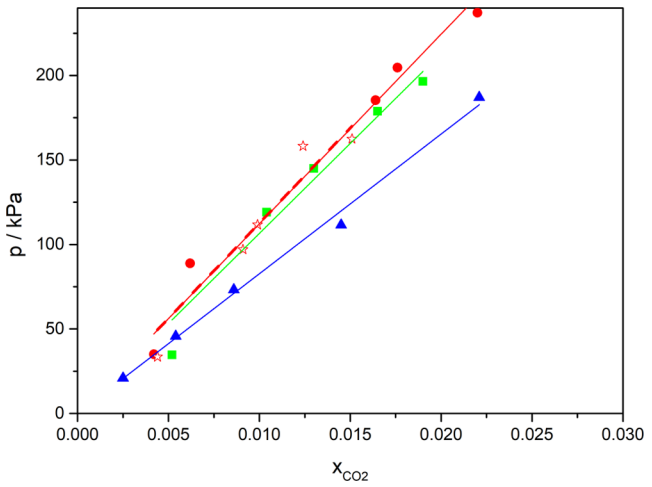

Figure 6. Solubility of carbon dioxide in studied DESs: circle, DES-A1; star, DES-A2; square, DES-B1; triangle, DES-C1; and lines, linear fit.

pressure (P), the liquid phase molality (m_{CO_2}), and the mole fraction of CO_2 (x_{CO_2}). As expected, it was observed that for each DES, the solubility of CO_2 increased with decreasing temperature and increasing pressure.

Literature reports indicate that the absorption of carbon dioxide in DESs based on 1,2-propanediol is purely physical.[46] Thus, the solubility was described in terms of Henry's law (eq 4) and the obtained results are presented in Table 6. Henry's constants for DES-containing choline chloride, i.e., DES-A1 and DES-A2, have already been reported by Chen et al.[46] However, the authors obtained values of 30.68 and 30.59 at 293.15 K, which are about 3 times higher than those obtained in this study. This can result from different DES volumes and the similar equilibration time in both studies.

As the volume of the sample increases, the time needed to reach equilibrium and to ensure the homogeneous saturation of the whole volume of the sample also increases. Higher volume results in the elongation of equilibration period due to longer time needed for gas molecules to diffuse in the whole volume of the liquid and pressure changes become slower with time, from our experience, even barely noticeable in the short time periods. Chen et al. reported the volume of equilibrium

Table 6. Henry's Law Constants (H_x) of CO_2 in the Studied DESs

DES	T/K	H_x/MPa
DES-A1	293.15	10.8 ± 0.36
	298.15	11.2 ± 0.39
	303.15	11.8 ± 0.44
	308.15	12.3 ± 0.51
	313.15	13.2 ± 0.58
DES-A2	293.15	10.7 ± 0.54
	298.15	11.1 ± 0.55
	303.15	11.9 ± 0.57
	308.15	12.8 ± 0.57
	313.15	13.4 ± 0.59
DES-B1	293.15	10.2 ± 0.40
	298.15	10.7 ± 0.40
	303.15	11.2 ± 0.42
	308.15	11.9 ±0.43
	313.15	12.7 ± 0.48
DES-C1	293.15	7.8 ± 0.21
	298.15	8.3 ± 0.18
	303.15	8.8 ± 0.26
	308.15	9.6 ± 0.35
	313.15	10.4 ± 0.51

cell of 141.61 cm^3 and they assumed that the system reached equilibrium when the pressure remained stable for 4 h.[46] From our experience, the time was not enough for the large volume system to ensure homogeneous saturation of the whole liquid column. In our methodology, equilibrium was considered to be reached when the pressure in the system did not change for 1 kPa over 24 h. Thus, a much lower solubility of CO_2 in the cited work may result from too short waiting time for reaching equilibrium. The correctness of our experimental procedure is also confirmed by the validation presented in the Supporting Information.

Comparison of Henry's constants values for DES-A1 and DES-A2 shows the effect of HBA/HBD molar ratio on carbon dioxide solubility in deep eutectic solvents. As can be seen from Table 6, for all temperatures and after consideration of experimental error, Henry's constants are undistinguishable. This indicates a similar solubility of CO_2 in CHCl:1,2-propanediol at a HBA/HBD molar ratio of 1:4 and 1:3.

When DESs with different salts are considered, depending on HBA, the solubility of CO_2 increases in the following order: ChCl:P (DES-A1) < AchCl:P (DES-B1) < TBAC:P (DES-C1) regardless of temperature. The higher CO_2 solubility observed by our group for DES based on acetylcholine chloride than for DES based on choline chloride is consistent with the literature.[47] The results obtained by Liu et al. for guaiacol-based DESs also showed a positive effect of the carboxylic group on the affinity for CO_2 compared to that of the hydroxyl group. The highest solubility of carbon dioxide in DES-containing TBAC seems to be related to the distinctly largest free volume (see Table 3) of this solvent, resulting from longer alkyl chains and greater symmetry of the TBAC molecule compared to the ChCl and ACC molecules.[48,49]

Permeability of Gases in DES-Based SLMs. The permeability of pure gases (CO_2 and N_2) in the synthesized SLMs was studied in the temperature range of 293.15−313.15 K, and the results along with the ideal selectivity α_{CO_2/N_2} are presented in Table 7.

https://doi.org/10.1021/acssuschemeng.2c06278
ACS Sustainable Chem. Eng. 2023, 11, 4093−4105

Table 7. Pure Gas Permeability and Ideal Selectivity

DES	T/K	P/barrer		
		CO_2	N_2	α_{CO_2/N_2}
DES-A1 (ChCl:1,2-propanediol 1:3)	293.15	86 ± 6.4	3 ± 0.3	29 ± 3.6
	298.15	104 ± 7.4	5 ± 0.4	21 ± 2.2
	303.15	117 ± 9.4	6 ± 0.5	19 ± 2.2
	308.15	130 ± 10.7	7 ± 0.5	19 ± 2.0
	313.15	145 ± 11.8	16 ± 1.2	9 ± 1.0
DES-A2 (ChCl:1,2-propanediol 1:4)	293.15	96 ± 6.7	4 ± 0.3	24 ± 2.5
	298.15	112 ± 8.0	5 ± 0.4	22 ± 2.4
	303.15	120 ± 8.5	8 ± 0.6	15 ± 1.5
	308.15	135 ± 10.1	10 ± 0.7	14 ± 1.4
	313.15	149 ± 11.5	23 ± 1.8	6 ± 0.7
DES-B1 (AchCl:1,2-propanediol 1:3)	293.15	117 ± 8.0	4 ± 0.3	29 ± 3.0
	298.15	127 ± 8.9	7 ± 0.5	18 ± 1.8
	303.15	141 ± 9.9	8 ± 0.6	18 ± 1.8
	308.15	154 ± 10.6	8 ± 0.7	19 ± 2.1
	313.15	170 ± 11.0	14 ± 1.1	12 ± 1.2
DES-C1 (TBAC:1,2-propanediol 1:3)	293.15	152 ± 9.3	5 ± 0.4	30 ± 3.1
	298.15	162 ± 10.4	8 ± 0.6	20 ± 2.0
	303.15	191 ± 13.8	14 ± 0.9	14 ± 1.3
	308.15	207 ± 14.6	24 ± 1.6	9 ± 0.8
	313.15	226 ± 17.0	29 ± 1.9	8 ± 0.8

The solution−diffusion theory (SDT) was found to be the most accepted model to explain gas transport through a membrane.[50] According to this theory, gas is first absorbed at the membrane feed side surface, then diffuses through the membrane, and finally is desorbed from the permeate side surface of the membrane. The driving force of this process is the gas chemical potential gradient over the membrane. The separation process depends on both the solubility of the gas in the liquid forming the membrane phase and the viscosity and free volume of the solvent. Both solubility and diffusivity determine permeability and selectivity.

Thus, the higher CO_2 permeability in the DES-based SLMs compared to N_2 (Table 7) is undoubtedly the result of the distinctly higher solubility of carbon dioxide in the studied DESs.

Solubility also determines the order of pure CO_2 permeability, which varies as follows: DES-C1 > DES-B1 > DES-A2 > DES-A1. This factor seems to be stronger than the viscosity effect because DES-C1, despite the highest viscosity, and the same highest diffusion resistance, has the highest permeability. The high permeability of this DES is favored not only by high solubility of CO_2 but also by its large free volume. The largest free volume of DES-C1 can compensate for the diffusion resistance associated with the high viscosity, resulting in the best permeability values. DES-B1, despite higher viscosity and lower free volume than DES-A1 and DES-A2, shows higher values of CO_2 permeability. This suggests a greater influence of the solubility of carbon dioxide in this DES than its properties responsible for diffusion resistance.

The permeability of N_2 is mainly due to the diffusion resistance since the solubility of N_2 in DESs is negligibly small.[51−54] In general, the values of N_2 permeability are the highest for DES-C1-based SLM at all temperatures, while for other DES-based SLMs the values of this parameter are similar, and their order is different from temperature. It seems that the free volume of DESs is mostly responsible for this behavior as its value is highest for DES-C1 and is similar for other DESs.

Effect of Temperature on Permeability of Gases in Synthesized DES-Based SLMs. As shown in Table 7, for all membranes, an increase in temperature results in an increase of the permeability of both carbon dioxide and nitrogen. This phenomenon may be due to the rapid decrease in DES viscosity with increasing temperature. At higher temperatures, the intermolecular interactions in DESs become weaker, resulting in lower diffusion resistance. This increases the mobility of free species in DES and consequently leads to their higher permeability. On the other hand, the solubility of gases decreases with increasing temperature, which would result in a decrease in permeability. However, since the permeability of CO_2 and N_2 increases with the increase of temperature, the solubility effect seems to be much less significant than that related to decreasing viscosity. This conclusion is consistent with the results obtained by other authors for the different DES and IL-based SLMs.[13,26,55,56] This effect is the most easily noticeable for DES-C1. Increase of temperature causes the drop of viscosity and the viscosity decreased at a faster rate for DES-C1, which has the highest viscosity of DESs used in this study. And for that mixture, the increase of N_2 permeability has the highest slope, corresponding to the decrease of viscosity. The permeability of CO_2 increases with temperature at approximately the same rate for all of DESs and it is in agreement with the viscosity and solubility values. Solubility decreases at the same rate for DES-A1, DES-A2, and DES-B1, and the highest decrease in the examined range is observed for DES-C1. The highest decrease of CO_2 solubility combined with the highest viscosity decrease results in similar CO_2 permeability increase rate.

The effect of temperature on the carbon dioxide permeability in the studied DES−SLMs is presented in Figure 7. As can be seen, all DES−SLMs show Arrhenius behavior in terms of CO_2 permeability in the studied temperature range with the coefficient of determination (R^2) close to 0.99. The Arrhenius equation explains the relationship between temperature and permeation using activation energy and is given as

https://doi.org/10.1021/acssuschemeng.2c06278
ACS Sustainable Chem. Eng. 2023, 11, 4093−4105

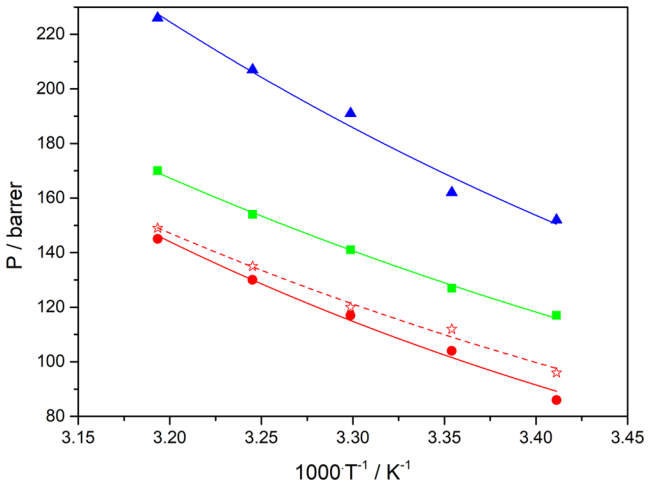

Figure 7. Arrhenius plot of temperature and CO_2 permeability; squares are experimental values, while solid lines are calculated by the Arrhenius equation; circle, DES-A1; star, DES-A2; square, DES-B1; and triangle, DES-C1.

$$P = P_0 e^{-E_a/RT} \quad (8)$$

where P is the permeability of CO_2, P_0 is the pre-exponential coefficient, R is the gas constant, T is the temperature, and E_a is the activation energy.

The activation energies of permeation were found to be 18.85, 16.17, 14.45, and 15.78 kJ·mol^{-1} for DES-A1, DES-A2, DES-B1, and DES-C1, respectively. They are therefore between for the earlier reported SLMs using different commercial polymeric supports based on DESs consisting of choline chloride and alkanoamines or acids and SLMs based on ILs containing acetic anion.[13,23,25,55] According to the literature, this may be due to many reasons, including differences in the viscosity of solvents and the porosity of solid materials in SLM.[13,55]

Selectivity of Studied Membranes. The ideal CO_2/N_2 selectivity values were calculated from eq 6 and are presented in Table 7 and Figure 8. As can be seen from eq 6, the ideal CO_2/N_2 selectivity of membranes is strictly connected to the permeability of pure gases.

Temperature has a great effect on all physical properties of DESs and by that on ideal CO_2/N_2 selectivity. As can be seen from Figure 8, the effect of temperature on α_{CO_2/N_2} is complex. For the ease of discussion, Figure 8 has been divided into four segments. In general, the ideal CO_2/N_2 selectivity decreases with an increase of temperature for all systems studied because the solubility-driven permeability of CO_2 increases at lower rate than the diffusion-driven permeability of N_2. For DES-C1-based SLMs, the ideal CO_2/N_2 selectivity decreases exponentially from segments I–IV, while for DES-A1 and DES-B1 is decreasing exponentially from segments I–III and then drops harshly in segment IV.

In the first segment, α_{CO_2/N_2} order is as follows: DES-B1 > DES-C1 > DES-A1 > DES-A2. The lowest values of α_{CO_2/N_2} for DES-A2 are due to its relatively low permeability of CO_2 and medium permeability of N_2 in comparison to other membranes studied in this work. This can be a combined result of the lowest viscosity of DES-A2 and low free volume values. The similar values of ideal CO_2/N_2 selectivity for DES-B1 and DES-C1 could be due to the compensation of high CO_2 solubility values in DES-C1 with its high viscosity in comparison for DES-B1. The other important factor may be the highest differences in free volume in these two DESs, which have an impact on the permeability of both CO_2 and N_2.

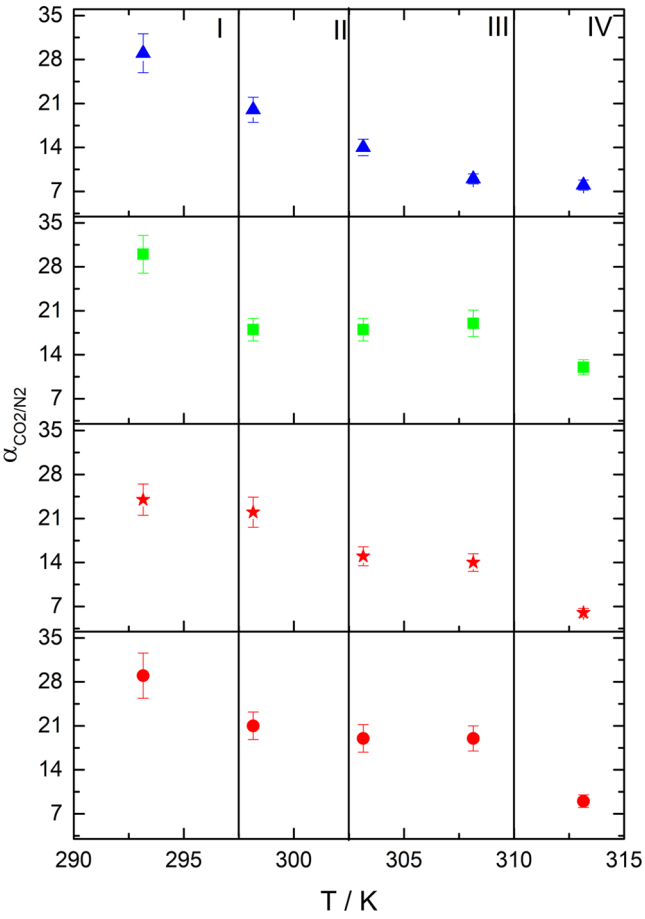

Figure 8. Experimental ideal CO_2/N_2 selectivity values as a function of temperature; circle, DES-A1; star, DES-A2; square, DES-B1; and triangle, DES-C1.

In the second segment, the ideal CO_2/N_2 selectivity values are close for all membranes studied. This is due to a high drop in viscosity for DES-B1 and DES-C1 and a relatively low decrease for DES-A1 and DES-A2. By that, the viscosity values of DES-A2 and DES-B2 are becoming similar to each other, which could explain similar behavior and values of selectivity.

In the third segment, α_{CO_2/N_2} of DES-A1 and DES-B1 is rather stable, whereas that of DES-A2 and DES-C1 is decreasing. The highest ideal CO_2/N_2 selectivity for DES-A1-based SLM is due its lowest CO_2 and N_2 permeability. The lowest values of selectivity obtained for DES-C1-based SLM might be due to the highest free volume values at that range.

In the last segment, α_{CO_2/N_2} order is as follows: DES-B1 > DES-A1 > DES-C2 > DES-A2. The shift between the order of the first two membranes might be due to the fact that both DESs have similar viscosity values at this temperature, but AChCl-based DES has lower free volume values and higher solubility of CO_2. The lowest values of ideal CO_2/N_2 selectivity for the DES-A2 based membrane are due to its lowest viscosity and lowest carbon dioxide solubility.

In general, its seems that the effect of temperature on the ideal CO_2/N_2 selectivity of DES-based SLM is mostly viscosity-driven, as the viscosity of DESs decreased at a higher

https://doi.org/10.1021/acssuschemeng.2c06278
ACS Sustainable Chem. Eng. 2023, 11, 4093–4105

rate than the solubility of CO_2. However, molar volume and CO_2 solubility also affect this parameter, suggesting a complex relationship between temperature and α_{CO_2/N_2}, which implies that all of these parameters must be taken into account when designing new membranes. At the examined range, the highest decrease of selectivity was observed for DES-C1, as both the viscosity and the CO_2 solubility drop were the highest. The lowest selectivity decrease was recorded for DES-B1, though the viscosity drop was comparable to DES-A1 and DES-A2, the CO_2 solubility decreased for most of the DESs studied.

Only a few DES-based supported liquid membranes were reported in the literature. Alkanolamine-based deep eutectic solvents reported by Ishaq et al. were characterized by lower permeabilities of CO_2 and N_2 but higher ideal selectivities than SLMs reported by our group. The higher ideal selectivities were also obtained by Saeed et al.[25] From results obtained by Craveiro *et al.*, in most cases, the values were similar to those reported in this study.[14] Selectivities obtained for ionic liquids are close to values obtained within this study. Scovazzo et al.[57] reported ideal selectivities for SILMs based on [emim][Tf_2N] and [C_6mim][Tf_2N] equal to 23 and 15, respectively. It proves that DES−SLMs can be a "greener" alternative for ionic liquid-based SLMs. It is worth mentioning that supported liquid membranes are not yet more efficient than traditional carbon dioxide removal methods. However, this work shows that DES-based SLMs are a great new research direction for more energy-efficient and less environmentally harmful methods.

CONCLUSIONS

The newly supported liquid membranes were prepared based on deep eutectic solvents composed of 1,2-propanediol combined with choline chloride, acetylcholine chloride, or tetrabutylammonium chloride. The physical properties, namely, thermal stability, density, viscosity, and refractive indices of DESs, were measured. In addition, FTIR spectra were recorded to confirm the formation of DESs. Solubility of carbon dioxide in studied DESs was examined and used for calculations of Henry's constants. The permeability values of pure carbon dioxide and nitrogen in DES-based SLMs were measured, and ideal CO_2/N_2 selectivities were determined.

It was found that both hydrogen bond acceptor type and molar ratio of HBA/HBD affect the physicochemical properties of DESs. The greatest differences were observed for the TBAC-based deep eutectic solvent. It was attributed to the presence of long alkyl chains in the TBAC molecule. It was also established that the type of HBA highly affects carbon dioxide solubility. The highest solubility was observer for TBAC-based DESs, while the lowest was observed for ChCl-based DESs. In addition, the molar ratio of HBA/HBA has a very little effect on CO_2 solubility.

The type of solvent used as well as its physical properties appeared to have a significant effect on the permeability of gases in the synthesized DES-based SLMs and by that on its selectivity. It was concluded that carbon dioxide solubility, free volume, and viscosity of deep eutectic solvents must be taken into account when considering DES potential for membrane separation. It was found that increasing the temperature results in a decrease of the viscosity of DESs at a higher rate than the solubility of CO_2, resulting in a higher rate of N_2 permeability increase over the CO_2 permeability, affecting the values of ideal selectivity. It appears that at lower temperatures the influence of CO_2 solubility predominates, while at higher temperatures the viscosity factor plays a key role in membrane selectivity.

ASSOCIATED CONTENT

Supporting Information

The Supporting Information is available free of charge at https://pubs.acs.org/doi/10.1021/acssuschemeng.2c06278.

Validation of the gas solubility method, fitting of physicochemical parameters, and experimental results of gas solubility (PDF)

(PDF)

(PDF)

AUTHOR INFORMATION

Corresponding Author

Iwona Cichowska-Kopczyńska − *Department of Process Engineering and Chemical Technology, Chemical Faculty, Gdańsk University of Technology, 80-233 Gdańsk, Poland;* orcid.org/0000-0003-3070-9603; Phone: +48583471869; Email: iwona.kopczynska@pg.edu.pl; Fax: +48583472065

Authors

Bartosz Nowosielski − *Department of Physical Chemistry, Chemical Faculty, Gdańsk University of Technology, 80-233 Gdańsk, Poland*

Dorota Warmińska − *Department of Physical Chemistry, Chemical Faculty, Gdańsk University of Technology, 80-233 Gdańsk, Poland*

Complete contact information is available at: https://pubs.acs.org/10.1021/acssuschemeng.2c06278

Notes

The authors declare no competing financial interest.

REFERENCES

(1) Keith, D. W. Why Capture CO2 from the Atmosphere? *Science* **2009**, *325*, 1654−1655.

(2) Song, C.; Liu, Q.; Deng, S.; Li, H.; Kitamura, Y. Cryogenic-Based CO2 Capture Technologies: State-of-the-Art Developments and Current Challenges. *Renewable Sustainable Energy Rev.* **2019**, *101*, 265−278.

(3) Yu, C. H.; Huang, C. H.; Tan, C. S. A Review of CO2 Capture by Absorption and Adsorption. *Aerosol Air Qual. Res.* **2012**, *12*, 745−769.

(4) Kenarsari, S. D.; Yang, D.; Jiang, G.; Zhang, S.; Wang, J.; Russell, A. G.; Wei, Q.; Fan, M. Review of Recent Advances in Carbon Dioxide Separation and Capture. *RSC Adv.* **2013**, *3*, 22739−22773.

(5) Scholes, C. A.; Stevens, G. W.; Kentish, S. E. Membrane Gas Separation Applications in Natural Gas Processing. *Fuel* **2012**, *96*, 15−28.

(6) Grünauer, J.; Shishatskiy, S.; Abetz, C.; Abetz, V.; Filiz, V. Ionic Liquids Supported by Isoporous Membranes for CO2/N2 Gas Separation Applications. *J. Membr. Sci.* **2015**, *494*, 224−233.

(7) Yan, X.; Anguille, S.; Bendahan, M.; Moulin, P. Ionic Liquids Combined with Membrane Separation Processes: A Review. *Sep. Purif. Technol.* **2019**, *222*, 230−253.

(8) Cichowska-Kopczyńska, I.; Aranowski, R. Use of Pyridinium and Pyrrolidinium Ionic Liquids for Removal of Toluene from Gas Streams. *J. Mol. Liq.* **2019**, No. 112091.

(9) Wang, J.; Luo, J.; Feng, S.; Li, H.; Wan, Y.; Zhang, X. Recent Development of Ionic Liquid Membranes. *Green Energy Environ.* **2016**, *1*, 43−61.

(10) Mubashir, M.; D'Angelo, F. N.; Gallucci, F. Recent Advances and Challenges of Deep Eutectic Solvent Based Supported Liquid Membranes. *Sep. Purif. Rev.* **2022**, *51*, 226−244.
(11) Patiño, J.; Gutiérrez, M. C.; Carriazo, D.; Ania, C. O.; Parra, J. B.; Ferrer, M. L.; Monte, F. Del. Deep Eutectic Assisted Synthesis of Carbon Adsorbents Highly Suitable for Low-Pressure Separation of CO 2-CH 4 Gas Mixtures. *Energy Environ. Sci.* **2012**, *5*, 8699−8707.
(12) Jiang, B.; Zhang, N.; Wang, B.; Yang, N.; Huang, Z.; Yang, H.; Shu, Z. Deep Eutectic Solvent as Novel Additive for PES Membrane with Improved Performance. *Sep. Purif. Technol.* **2018**, *194*, 239−248.
(13) Ishaq, M.; Gilani, M. A.; Bilad, M. R.; Faizan, A.; Raja, A. A.; Afzal, Z. M.; Khan, A. L. Exploring the Potential of Highly Selective Alkanolamine Containing Deep Eutectic Solvents Based Supported Liquid Membranes for CO2 Capture. *J. Mol. Liq.* **2021**, *340*, No. 117274.
(14) Craveiro, R.; Neves, L. A.; Duarte, A. R. C.; Paiva, A. Supported Liquid Membranes Based on Deep Eutectic Solvents for Gas Separation Processes. *Sep. Purif. Technol.* **2021**, *254*, No. 117593.
(15) Cichowska-Kopczyńska, I.; Warmińska, D.; Nowosielski, B. Solubility of Carbon Dioxide in Deep Eutectic Solvents Based on 3-Amino-1-Propanol and Tetraalkylammonium Salts at Low Pressure. *Materials* **2021**, *14*, No. 594.
(16) Xu, M.; Dou, H.; Peng, F.; Yang, N.; Xiao, X.; Tantai, X.; Sun, Y.; Jiang, B.; Zhang, L. Ultra-Stable Copper Decorated Deep Eutectic Solvent Based Supported Liquid Membranes for Olefin/Paraffin Separation: In-Depth Study of Carrier Stability. *J. Membr. Sci.* **2022**, *659*, No. 120775.
(17) Seyyed Shahabi, S.; Azizi, N.; Vatanpour, V. Tuning Thin-Film Composite Reverse Osmosis Membranes Using Deep Eutectic Solvents and Ionic Liquids toward Enhanced Water Permeation. *J. Membr. Sci.* **2020**, *610*, No. 118267.
(18) Castro-Muñoz, R.; Galiano, F.; Figoli, A.; Boczkaj, G. Deep Eutectic Solvents − A New Platform in Membrane Fabrication and Membrane-Assisted Technologies. *J. Environ. Chem. Eng.* **2022**, *10*, No. 106414.
(19) Taghizadeh, M.; Taghizadeh, A.; Vatanpour, V.; Ganjali, M. R.; Saeb, M. R. Deep Eutectic Solvents in Membrane Science and Technology: Fundamental, Preparation, Application, and Future Perspective. *Sep. Purif. Technol.* **2021**, *258*, No. 118015.
(20) Marcus, Y. *Deep Eutectic Solvents*; Springer International Publishing, 2019. DOI: 10.1007/978-3-030-00608-2.
(21) Amira, M. N.; Irfan Hatim, M. D.; Jullok, N.; Syahmie Rasidi, M.; Alamery, H. R. Synthesis and Preparation of Asymmetric PVDF-Co-PTFE/DES Supported Membrane for CO2/N2 Separation. *IOP Conf. Ser. Mater. Sci. Eng.* **2018**, *429*, No. 012067.
(22) Ishaq, M.; Gilani, M. A.; Ahmad, F.; Afzal, Z. M.; Arshad, I.; Bilad, M. R.; Ayub, K.; Khan, A. L. Theoretical and Experimental Investigation of CO2 Capture through Choline Chloride Based Supported Deep Eutectic Liquid Membranes. *J. Mol. Liq.* **2021**, *335*, No. 116234.
(23) Ishaq, M.; Gilani, M. A.; Afzal, Z. M.; Bilad, M. R.; Nizami, A. S.; Rehan, M.; Tahir, E.; Khan, A. L. Novel Poly Deep Eutectic Solvents Based Supported Liquid Membranes for CO2 Capture. *Front. Energy Res.* **2020**, *8*, No. 595041.
(24) Saeed, U.; Khan, A. L.; Gilani, M. A.; Aslam, M.; Khan, A. U. CO2 Separation by Supported Liquid Membranes Synthesized with Natural Deep Eutectic Solvents. *Environ. Sci. Pollut. Res.* **2021**, *28*, 33994−34008.
(25) Saeed, U.; Khan, A. L.; Gilani, M. A.; Bilad, M. R.; Khan, A. U. Supported Deep Eutectic Liquid Membranes with Highly Selective Interaction Sites for Efficient CO2 Separation. *J. Mol. Liq.* **2021**, *342*, No. 117509.
(26) Saeed, U.; Khan, A. U.; Khan, A. L.; Gilani, M. A.; Bilad, M. R. Separation of Carbon Dioxide by Potassium Carbonate Based Supported Deep Eutectic Liquid Membranes: Influence of Hydrogen Bond Donor. *J. Membr. Sci. Res.* **2022**, *8*, No. 526587.
(27) Lian, S.; Li, R.; Zhang, Z.; Liu, Q.; Song, C.; Lu, S. Improved CO2 Separation Performance and Interfacial Affinity of Composite Membranes by Incorporating Amino Acid-Based Deep Eutectic Solvents. *Sep. Purif. Technol.* **2021**, *272*, No. 118953.
(28) Castro, A. M. de.; Prasavath, D.; Bevilaqua, J. V.; Portugal, C. A. M.; Neves, L. A.; Crespo, J. G. Role of Water on Deep Eutectic Solvents (DES) Properties and Gas Transport Performance in Biocatalytic Supported DES Membranes. *Sep. Purif. Technol.* **2021**, *255*, No. 117763.
(29) Cichowska-Kopczyńska, I.; Aranowski, R. Effectiveness of Toluene Separation from Gas Phase Using Supported Ammonium Ionic Liquid Membrane. *Chem. Eng. Sci.* **2020**, *219*, No. 115605.
(30) Fortunato, R.; Afonso, C. A. M.; Reis, M. A. M.; Crespo, J. G. Supported Liquid Membranes Using Ionic Liquids: Study of Stability and Transport Mechanisms. *J. Membr. Sci.* **2004**, *242*, 197−209.
(31) Hernández-Fernández, F. J.; de los Ríos, A. P.; Tomás-Alonso, F.; Palacios, J. M.; Víllora, G. Preparation of Supported Ionic Liquid Membranes: Influence of the Ionic Liquid Immobilization Method on Their Operational Stability. *J. Membr. Sci.* **2009**, *341*, 172−177.
(32) Jia, T.; Bi, S.; Wu, J. Solubilities of Carbon Dioxide, Oxygen, and Nitrogen in Aqueous Ethylene Glycol Solution under Low Pressures. *Fluid Phase Equilib.* **2019**, *485*, 16−22.
(33) Praumitz, J.; Azevedo, E. G.; Lichtenthaler, R. *Molecular Thermodynamics of Fluid-Phase Equilibria*, 2nd ed.; Prentice-Hall Inc.: Englewood Cliffs: New Jersey, 1986.
(34) Lu, M.; Han, G.; Jiang, Y.; Zhang, X.; Deng, D.; Ai, N. Solubilities of Carbon Dioxide in the Eutectic Mixture of Levulinic Acid (or Furfuryl Alcohol) and Choline Chloride. *J. Chem. Thermodyn.* **2015**, *88*, 72−77.
(35) Liu, F.; Chen, W.; Mi, J.; Zhang, J. Y.; Kan, X.; Zhong, F. Y.; Huang, K.; Zheng, A. M.; Jiang, L. Thermodynamic and Molecular Insights into the Absorption of H2S, CO2, and CH4 in Choline Chloride plus Urea Mixtures. *AIChE J.* **2019**, *65*, No. e16574.
(36) Ghaedi, H.; Ayoub, M.; Sufian, S.; Lal, B.; Uemura, Y. Thermal Stability and FT-IR Analysis of Phosphonium-Based Deep Eutectic Solvents with Different Hydrogen Bond Donors. *J. Mol. Liq.* **2017**, *242*, 395−403.
(37) Ullah, R.; Atilhan, M.; Anaya, B.; Khraisheh, M.; García, G.; Elkhattat, A.; Tariq, M.; Aparicio, S. A Detailed Study of Cholinium Chloride and Levulinic Acid Deep Eutectic Solvent System for CO2capture via Experimental and Molecular Simulation Approaches. *Phys. Chem. Chem. Phys.* **2015**, *17*, 20941−20960.
(38) Al-Badr, A. A.; El-Obeid, H. A. Acetylcholine Chloride: Physical Profile. *Profiles Drug Subst., Excipients, Relat. Methodol.* **2005**, *31*, 1−19.
(39) Majid, M. F.; Mohd Zaid, H. F.; Kait, C. F.; Ghani, N. A.; Jumbri, K. Mixtures of Tetrabutylammonium Chloride Salt with Different Glycol Structures: Thermal Stability and Functional Groups Characterizations. *J. Mol. Liq.* **2019**, *294*, No. 111588.
(40) Dias, M. C. G. C.; Farias, F. O.; Gaioto, R. C.; da Costa, M. C.; Igarashi-Mafra, L.; Mafra, M. R. The Feasibility of the Alcohol-Based Deep Eutectic Solvents: From Thermophysical Characterization to Application in Active Pharmaceutical Ingredients Systems. *J. Solution Chem.* **2022**, *51*, 577−593.
(41) Vuksanović, J.; Kijevčanin, M. L.; Radović, I. R. Effect of Water Addition on Extraction Ability of Eutectic Solvent Choline Chloride+1,2-Propanediol for Separation of Hexane/Heptane+ethanol Systems. *Korean J. Chem. Eng.* **2018**, *35*, 1477−1487.
(42) Gajardo-Parra, N. F.; Cotroneo-Figueroa, V. P.; Aravena, P.; Vesovic, V.; Canales, R. I. Viscosity of Choline Chloride-Based Deep Eutectic Solvents: Experiments and Modeling. *J. Chem. Eng. Data* **2020**, *65*, 5581−5592.
(43) Rodriguez Rodriguez, N.; Machiels, L.; Binnemans, K. P -Toluenesulfonic Acid-Based Deep-Eutectic Solvents for Solubilizing Metal Oxides. *ACS Sustainable Chem. Eng.* **2019**, *7*, 3940−3948.
(44) Abbott, A. P.; Capper, G.; Gray, S. Design of Improved Deep Eutectic Solvents Using Hole Theory. *ChemPhysChem* **2006**, *7*, 803−806.
(45) Ghaedi, H.; Ayoub, M.; Sufian, S.; Lal, B.; Shariff, A. M. Measurement and Correlation of Physicochemical Properties of Phosphonium-Based Deep Eutectic Solvents at Several Temperatures

(293.15 K−343.15 K) for CO2 Capture. *J. Chem. Thermodyn.* **2017**, *113*, 41−51.
(46) Chen, Y.; Ai, N.; Li, G.; Shan, H.; Cui, Y.; Deng, D. Solubilities of Carbon Dioxide in Eutectic Mixtures of Choline Chloride and Dihydric Alcohols. *J. Chem. Eng. Data* **2014**, *59*, 1247−1253.
(47) Liu, X.; Gao, B.; Jiang, Y.; Ai, N.; Deng, D. Solubilities and Thermodynamic Properties of Carbon Dioxide in Guaiacol-Based Deep Eutectic Solvents. *J. Chem. Eng. Data* **2017**, *62*, 1448−1455.
(48) Zubeir, L. F.; Lacroix, M. H. M.; Kroon, M. C. Low Transition Temperature Mixtures as Innovative and Sustainable CO2 Capture Solvents. *J. Phys. Chem. B* **2014**, *118*, 14429−14441.
(49) Haider, M. B.; Jha, D.; Marriyappan Sivagnanam, B.; Kumar, R. Thermodynamic and Kinetic Studies of CO2 Capture by Glycol and Amine-Based Deep Eutectic Solvents. *J. Chem. Eng. Data* **2018**, *63*, 2671−2680.
(50) Wijmans, J. G.; Baker, R. W. The Solution-Diffusion Model: A Review. *J. Membr. Sci.* **1995**, *107*, 1−21.
(51) Li, Z. L.; Zhong, F. Y.; Huang, J. Y.; Peng, H. L.; Huang, K. Sugar-Based Natural Deep Eutectic Solvents as Potential Absorbents for NH3 Capture at Elevated Temperatures and Reduced Pressures. *J. Mol. Liq.* **2020**, *317*, No. 113992.
(52) Cheng, N.-N.; Li, Z.-L.; Lan, H.-C.; Xu, W.-L.; Jiang, W.-J.; Huang, K.; Peng, H.-L. Deep Eutectic Solvents with Multiple Weak Acid Sites for Highly Efficient, Reversible and Selective Absorption of Ammonia. *Sep. Purif. Technol.* **2021**, *269*, No. 118791.
(53) Jiang, W. J.; Zhang, J. B.; Zou, Y. T.; Peng, H. L.; Huang, K. Manufacturing Acidities of Hydrogen-Bond Donors in Deep Eutectic Solvents for Effective and Reversible NH3Capture. *ACS Sustainable Chem. Eng.* **2020**, *8*, 13408−13417.
(54) Liu, B.; Tian, J. Investigation of Glycolic Acid Natural Deep Eutectic Solvents with Strong Proton Donors for Ammonia Capture and Separation. *Ind. Eng. Chem. Res.* **2021**, *60*, 11600−11610.
(55) Santos, E.; Albo, J.; Irabien, A. Acetate Based Supported Ionic Liquid Membranes (SILMs) for CO2 Separation: Influence of the Temperature. *J. Membr. Sci.* **2014**, *452*, 277−283.
(56) Jindaratsamee, P.; Shimoyama, Y.; Morizaki, H.; Ito, A. Effects of Temperature and Anion Species on CO2 Permeability and CO2/N2 Separation Coefficient through Ionic Liquid Membranes. *J. Chem. Thermodyn.* **2011**, *43*, 311−314.
(57) Scovazzo, P.; Havard, D.; McShea, M.; Mixon, S.; Morgan, D. Long-Term, Continuous Mixed-Gas Dry Fed CO2/CH4 and CO2/N2 Separation Performance and Selectivities for Room Temperature Ionic Liquid Membranes. *J. Membr. Sci.* **2009**, *327*, 41−48.

https://doi.org/10.1021/acssuschemeng.2c06278
ACS Sustainable Chem. Eng. 2023, 11, 4093−4105